JOURNAL OF PROPULSION AND POWER
Vol. 18, No. 2, March–April 2002

Computations of Axisymmetric Plug-Nozzle Flowfields: Flow Structures and Thrust Performance

Takashi Ito*
University of Tokyo, Tokyo 113-8654, Japan
Kozo Fujii†
Institute of Space and Astronautical Science, Kanagawa 229-8510, Japan
and
A. Koich Hayashi‡
Aoyama Gakuin University, Tokyo 157-8572, Japan

Plug-nozzle flowfields are analyzed by the numerical simulations. The method of characteristics is used to design the plug contour, and several types of plug nozzles are considered by truncating the length of the nozzle at different positions. Plug-nozzles' altitude-compensating features are confirmed by the computed results, and the base pressure turns out to play an important role to maintain the thrust performance of the nozzle for high-truncation configurations. The altitude clearly influences the base-pressure distributions under the assumption that the chamber pressure is constant during the ascent. The computed thrust difference between the contoured and the conical nozzle linearly increased as a function of the pressure ratio. The thrust performance of the contoured plug nozzle is estimated to be about 5–6% higher than the conical plug nozzle. Various conditions of external flows over the plug nozzle are also imposed, and the result shows that the external flow does not influence the pressure distribution on the nozzle surface for the pressure ratios higher than the designed point.

Nomenclature

C_F = thrust coefficient
P = pressure
S = distance along the vehicle
Y = vertical coordinate
ϕ = plug exit half-angle

Subscripts

a = ambient condition
b = plug base
t = throat

Introduction

SINGLE-STAGE-TO-ORBIT (SSTO) rocket vehicles are expected to be main launching vehicles in the new future. It is believed to reduce the costs of the missions because of its full reusability and the mechanical simplicity (because of a "single stage"). A highly efficient propulsion system is one of the key factors to realize a SSTO. A plug nozzle seems to be a good candidate for that system, and it is widely studied in the last several years. Unlike a bell-shaped nozzle, the nozzle flow is not fixed by a wall, but, instead, the exhausted jet is bounded by the external flow. The plug nozzle is considered to have globally better performance because the jet boundary adjusts its shape to an ambient pressure, and the jet expands optimally for the entire conditions (e.g., altitude). In addition, the nozzle performance is believed not to be strongly affected by cutting off the nozzle because the base pressure compensates the loss of the thrust force. These favorable features of plug nozzles were confirmed by previous studies,[1–8] but the quantitative discussion was insufficient for the axisymmetric plug-nozzle configurations as a result of the limited number of experimental or computational results.

In the present research plug-nozzle flowfields are computationally simulated for the qualitative investigation of the preceding features. Two parameters, the chamber-to-ambient pressure ratio (PR) and the length of the nozzle, are systematically changed. To validate the numerical simulations, the results are compared with experiments[6] at several PRs. The flow structures are investigated, and the thrust performance is evaluated quantitatively.

A study of an optimum nozzle shape is another objective. The method of characteristics[9] is used for the design of the nozzle contour. The performance of the contoured-plug nozzle is compared with a simple conical plug nozzle.

The effect of the external flow over the plug nozzle is also investigated. Pressure ratio and external flow are systematically changed, and the performance of the pressure thrust produced at the nozzle surface is discussed.

First, an annular-type conical plug having a $\phi = 25$ deg half-angle[6] is used for the validation of the present computations. Three values of PRs—6, 15, and 340—are used for the comparison with experiments. Second, detailed analysis of the plug-nozzle performance is carried out using the plug nozzle designed by the method of characteristics.[9] Both the primary nozzle and external expansion region of the nozzle is designed by this method (Fig. 1, upper half). The comparison of the performance of the truncated nozzles is made for five types of plug nozzles truncated at 20, 30, 40, 50, and 100% portion of the total plug length (Fig. 2). The contoured nozzle has a conical portion from the discharge to the intersection of the first characteristic line from the cowl lip. The genuinely conical nozzle was intentionally created by linearly extending the conical portion of the contoured nozzle (see Fig. 3), and computations were carried out to see the performance improvement by the contoured nozzle. The area ratio (AR) for all types of plug nozzles is set to be the same. The ARs for the primary nozzle and the whole nozzle are 1.7 and 6.5, respectively. Optimum expansion is achieved at PR = 71

Presented as Paper 99-3211 at the 17th Applied Aerodynamics Conference, Norfolk, VA, 28 June–1 July 1999; received 5 February 2000; revision received 22 December 2000; accepted for publication 17 October 2001.

*Graduate Student, Department of Aeronautics and Astronautics, 7-3-1 Hongo, Bunkyo-Ku. Member AIAA.
†Professor, Yoshinodai 3-1-1, Sagamihara. Associate Fellow AIAA.
‡Professor, Department of Mechanical Engineering, Chitosedai 6-16-1, Setagaya. Member AIAA.

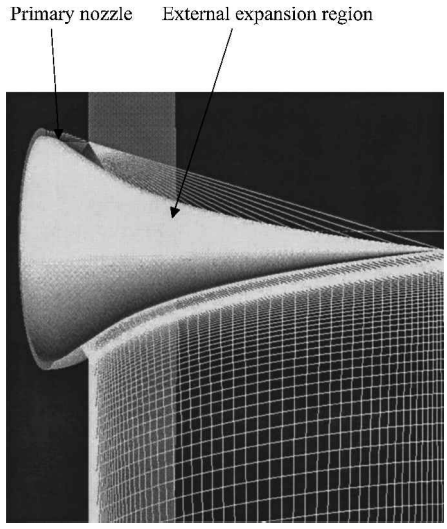

Fig. 1 Characteristic lines (upper half) and the grid distributions (lower half).

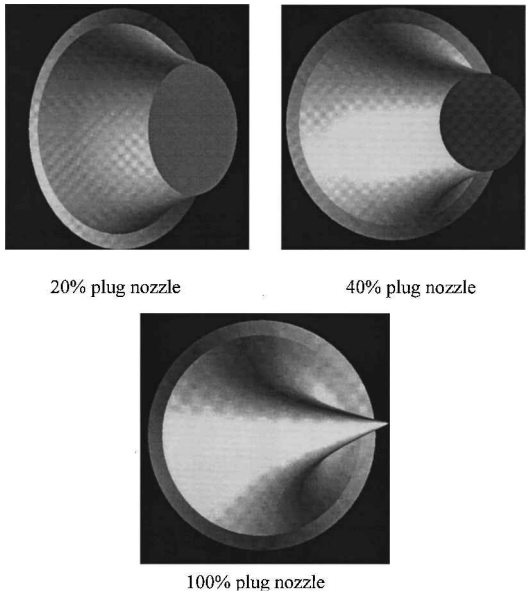

Fig. 2 Configurations of the truncated contoured plug nozzles.

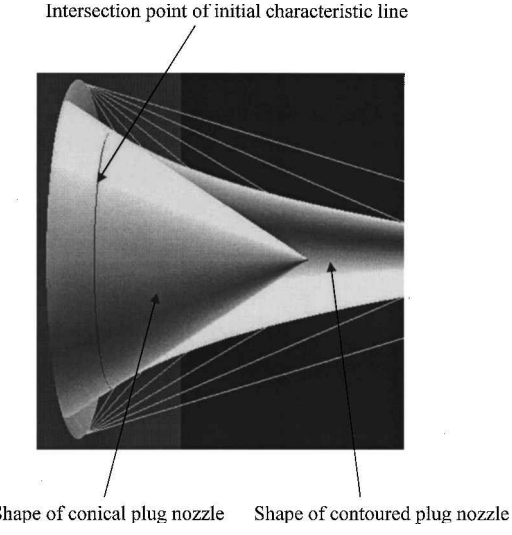

Fig. 3 Comparison of configuration of the conical and contoured plug nozzle.

under the assumption that the flow is isentropic. The PR and the external flow Mach number are systematically changed for the investigation of the effect of the external flow. The flowfield and the thrust characteristics, at PRs from 5 to 1000, are studied. The external flow Mach number is varied in the range from 0.0 to 3.4. The Reynolds number is set to 5×10^5 based on the length between the plug axis and cowl lip. The pressure is normalized by the sea-level pressure. Therefore all of the calculated parameters are based on this nondimensionalized pressure.

Numerical Method

The basic equations are three-dimensional Navier–Stokes equations. The flowfield inside the nozzle is computed in advance using the Euler equations, and the solution gives the flow conditions at the primary nozzle exit. The convective terms are evaluated by the simple high-resolution upwind scheme,[10] which is a family of advection-upwind-splitting-method type schemes. High-order space accuracy is obtained using monotonic upwind schemes for conservation laws for the primitive variable interpolation. The viscous terms are evaluated by the central differencing, and the eddy viscosity is modeled by the Baldwin–Lomax turbulence model[11] with the Degani–Schiff correction[12] implemented. Only the steady-state solutions are considered, and the Lower Upper-Alternate Directional Implicit factorization time-integration algorithm[13] is used. The flow is assumed to be axisymmetric, although three-dimensional equations are used for the future studies. Therefore, three points are distributed in the circumferential direction, and the solutions at all the three planes coincide at the steady state. The computational grid for the primary nozzle consists of 201 nodes in the streamwise direction and 51 nodes from the plug surface to the outer contour of the primary nozzle. For the external expansion region the computational grid consists of 151 nodes in the streamwise direction and 151 nodes from the plug surface to the outer boundary of the computational domain. Figure 1 (lower half) shows the grid distributions near the surface of the 100% plug nozzle.

Computed Results

Comparison of the Experimental and Numerical Results

Figures 4a, 5a, and 6a show the Mach-number distributions (upper half) and Mach-number contour plots (lower half) for the PRs 6, 15, and 340, respectively. Figures 4b, 5b, and 6b present the nondimensional pressure distributions along the nozzle surface for the same PRs. The horizontal axis is nondimensionalized by the length from the throat to the plug tip along its surface. $S = -1.0$ indicates the position at the throat, and $S = 0.0$ indicates the position at the plug tip.

For a PR equal to 6 in Fig. 4a, the primary nozzle is overexpanded, and therefore an oblique shock wave from the cowl lip is observed. The pressure increase caused by this shock wave is observed at $S = -0.8$ to -0.65 in the pressure distribution in Fig. 4b.

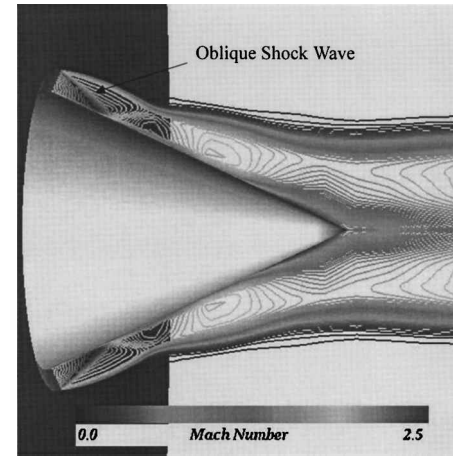

Fig. 4a Mach-number distributions (PR = 6).

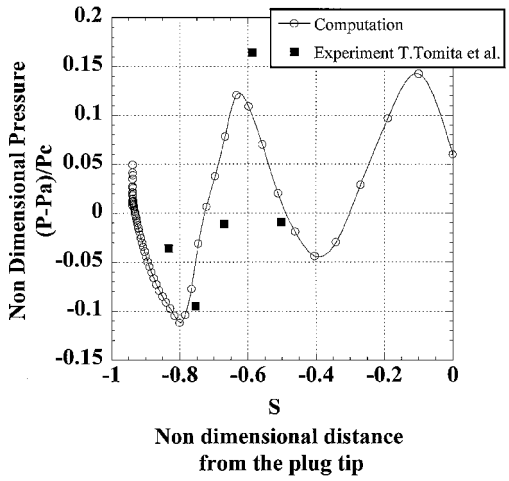

Fig. 4b Pressure profiles on the nozzle surface (PR = 6).

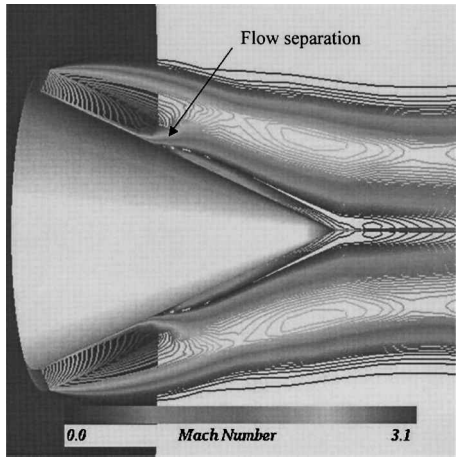

Fig. 5a Mach-number distributions (PR = 15).

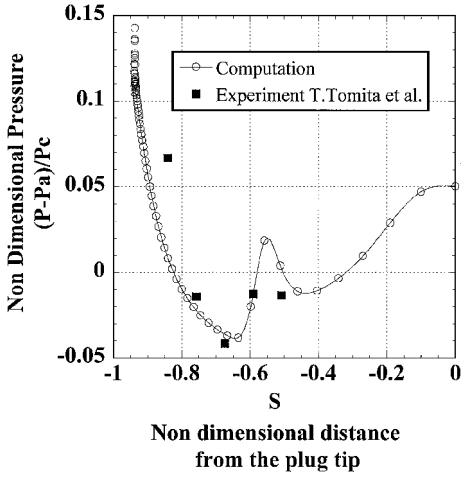

Fig. 5b Pressure profiles on the nozzle surface (PR = 15).

In Fig. 5a flow separation can be observed as a result of the over-expansion along the nozzle surface. The flow does not reattach to the nozzle surface after the separation. From the pressure distributions in Fig. 5b, the flow expands until it reaches $S = -0.63$. An abrupt pressure increase is caused by a separation shock wave.

In Fig. 6a strong expansion of the jet from the high PR is observed. The trailing shock from the plug tip is formed by the flow interaction. From the pressure distributions in Fig. 6b, no separation occurs, and the pressure decreases smoothly. The slight pressure increase observed at $S = 0.0$ is caused by the trailing shock wave.

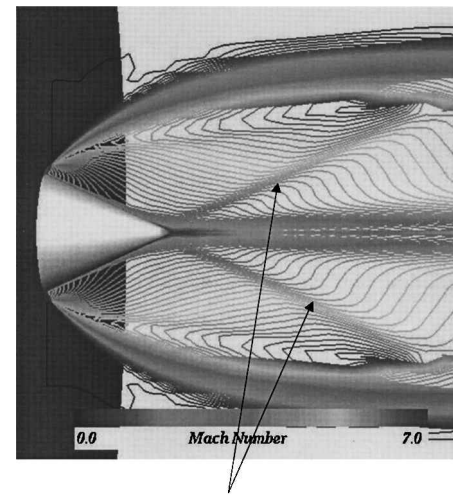

Fig. 6a Mach-number distributions (PR = 340).

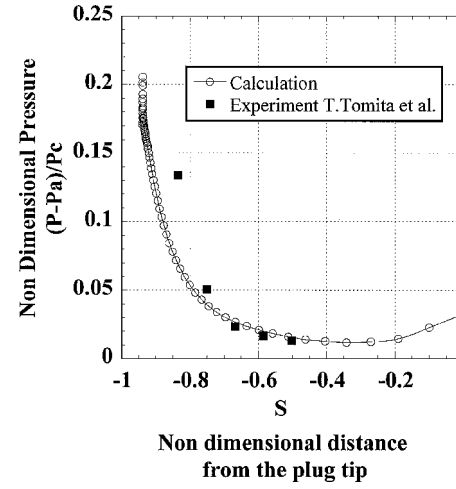

Fig. 6b Pressure profiles on the nozzle surface (PR = 340).

The pressure distributions in the experiment[6] are also plotted in Figs. 4b–6b. The computed results agree well with the experiment for all of the three PRs.

Flow Structures for the Various Pressure Ratios

The following discussion is made for the contoured plug nozzles. Figure 7 shows the pressure distribution (upper half) and the Mach-number contour plots (lower half) for the 100% plug nozzle at the design PR of 71. The pressure contours agree well with the characteristic lines shown in Fig. 1 (upper half). Because the PR is at its design point, the outer jet boundary is parallel to the plug axis (as shown in the Mach contour plots in Fig. 7 lower half), and the flow is at its optimum expansion.

Figures 8–10 show the Mach-number contour plots of the 20% (80% truncated) plug nozzle at the PRs 9, 71, and 500, respectively. In Fig. 8 the jet boundary becomes narrow as the PR of 9 is lower than the design point and the ambient pressure presses the jet boundary towards the nozzle surface. The jet also does not expand so much at the truncated portion on the plug, and the separation flow from the corner forms relatively large wake region compared with the flowfields of higher PRs at the base region. In Fig. 9 the outer jet boundary is not disturbed by the truncation of the nozzle, and the outer boundary of the jet flow is parallel to the axis. The trailing shock can be observed downstream of the base region because the jet expands at the truncated portion of the nozzle and converges at the axis. In Fig. 10 strong expansion of the jet caused by the high PR can be observed. A trailing shock wave is observed by the same

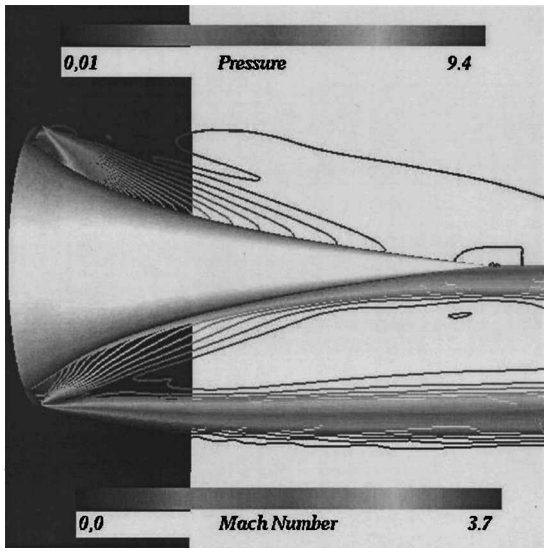

Fig. 7 Contour plots of pressure (upper half) and Mach-number (lower half) distributions (PR = 71).

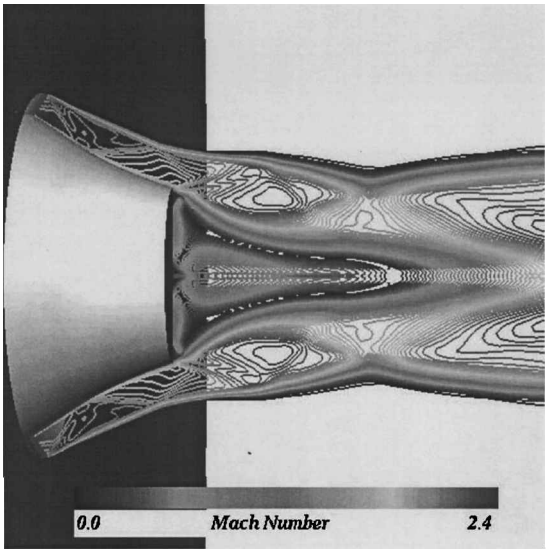

Fig. 8 Mach-number distributions (PR = 9).

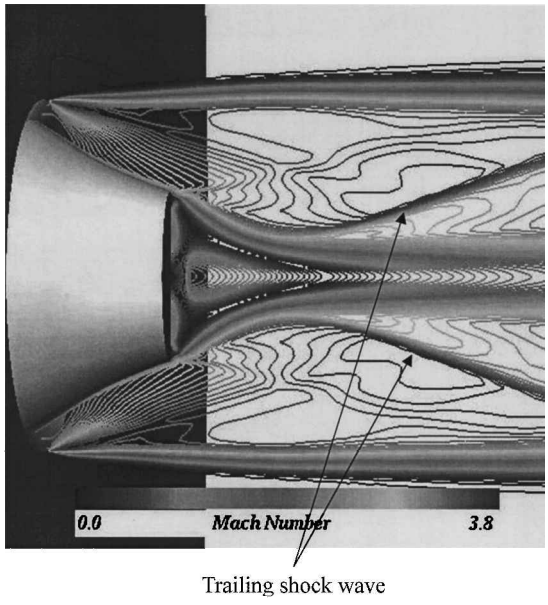

Fig. 9 Mach-number distributions (PR = 71).

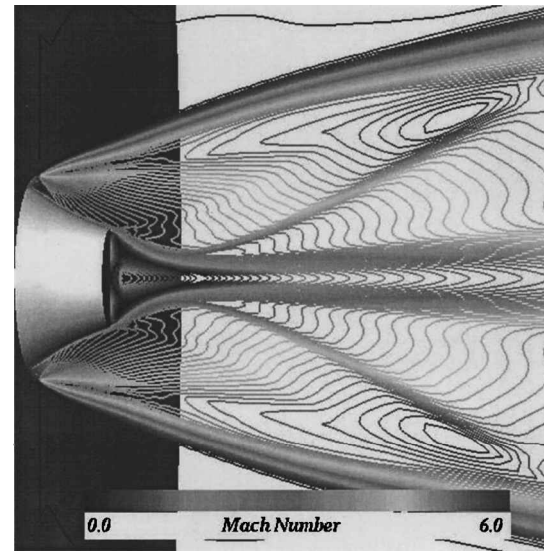

Fig. 10 Mach-number distributions (PR = 500).

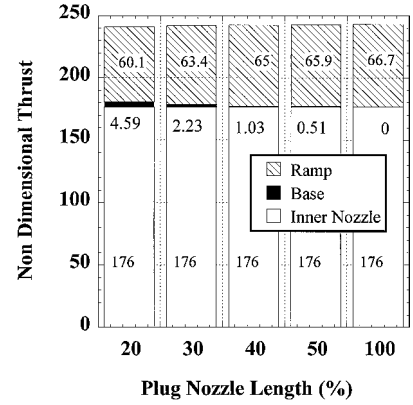

Fig. 11 Proportion of the thrust for each truncated nozzle at the PR of 500.

reason as in Fig. 9. In Figs. 8–10 the expansion boundary reflects the ambient pressure (PR effect). The capability of the plug nozzle to accommodate with the ambient pressure (altitude compensation) can be clearly observed.

Effect of Truncating the Plug

The effect of truncating the plug can be evaluated by the comparison of Fig. 7 (lower half) and Fig. 9 (lower half). For 100% nozzle the flow follows the nozzle wall and smoothly moves to the wake region. On the other hand, for the truncated nozzle the flow separates at the trailing edge and expands. The resulting shear longer induces the trailing shock wave when it converges and turns the flow parallel to the axis.

Analysis of the Thrust Performance

Figure 11 shows the portion of the thrust produced by each component of the plug nozzle at the PR of 500. When the plug is truncated, the nozzle length becomes shorter, and the ramp area for the nozzle decreases. Therefore the pressure thrust produced at the ramp reduces. On the other hand, the thrust generated by the base pressure increases as a result of the increase of the base area. It compensates the total thrust loss caused by the decrease of the ramp pressure thrust. Accordingly, the total nozzle thrust becomes almost the same for any nozzle truncation.

Investigation of supersonic base flows for the axisymmetric backward-facing step configurations provides valuable information for the estimation of the base pressure and resultantly for the prediction of thrust performance of truncated plug nozzles. To

confirm the reliability of the present simulations, backward-facing step flowfields used in Ref. 14 are computed by the same code as is used in the present paper. Although the result is not shown here, the averaged base pressure agreed well with Paciorri's computational result[14] obtained with the Spallart–Allmaras turbulence model.[15] Both the numerical results underpredict the base pressure roughly 50% compared to the experiments by Sykes,[16] Herrin and Dutton,[17] and Seiling and Page.[18] As the base pressure of the plug nozzle might be underestimated in the present study, the contribution of the base pressure might be larger but never be smaller to the total thrust.

Figure 12 shows the C_F of the 20% plug nozzle plotted against the PR. The solid line denotes the ideal C_F, and the dashed line denotes the theoretical C_F of the bell nozzle with the same PR as the plug nozzle. It is the theoretical value that can be achieved when optimum. In the low-PR region the bell nozzle does not produce as much thrust as the plug nozzle. That is the reason for higher performance of the plug nozzle at low PRs (lower altitudes). Qualitatively, C_F of the plug nozzle have the same trend as the ideal C_F, which indicates that the plug nozzle operates at nearly peak thrust efficiency in the wide range of the PR than the classical bell nozzle.

Figure 13 shows the averaged base pressure for the 20, 30, 40, and 50% plug nozzle plotted vs various PRs. This figure is plotted under the assumption that the vehicle's chamber pressure is constant during the ascent and five times higher than the atmospheric pressure at the sea level. The solid line shows the ambient pressure, which decreases as the PR or the altitude becomes higher. At the low altitudes (e.g., low-PR region) the base pressure linearly decreases as the ambient pressure decreases. In this region the jet does not converge, and the base region is opened to the external environment. Therefore, the base region is influenced by the external environment, and the pressure on the base quantitatively equals the ambient pressure. The pressure thrust that is produced by the pressure difference between the environment and the base becomes small at low altitudes.

On the other hand, at high altitudes the pressure on the base becomes constant despite the variation of the altitude. In the high-PR region the jet expands and converges downstream on the axis. Therefore the base region is closed, and the base pressure becomes independent from the external conditions. As the altitude becomes higher, the ambient pressure decreases, and the difference between the base pressure and the ambient pressure increases. Therefore the base pressure thrust increases.

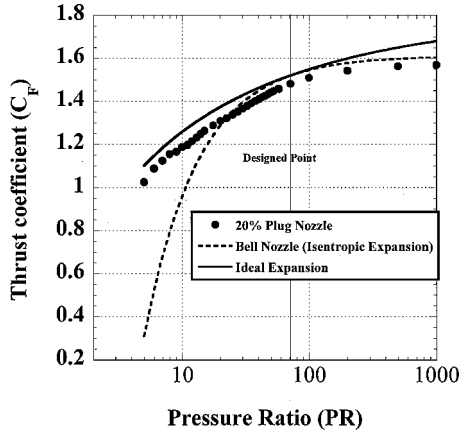

Fig. 12 Relation of the C_F to the PR.

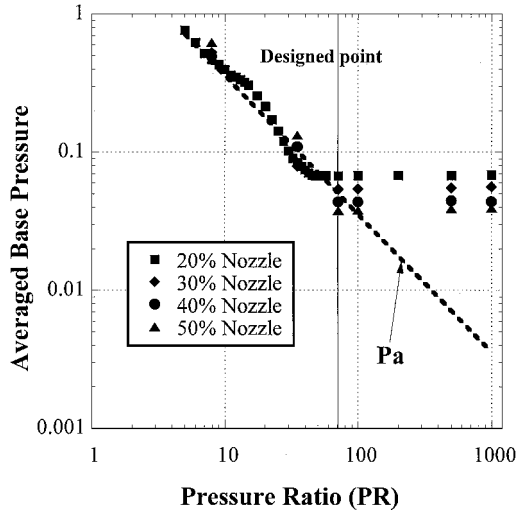

Fig. 13 Relation of the base pressure to the PR.

Comparison of the Nozzle Shape

Figure 14 shows the comparison of the pressure thrust of the contoured plug nozzle and the conical plug nozzle. The contoured plug nozzle has a higher performance than the conical plug nozzle for all of the PRs.

Figure 15 shows the pressure thrust difference between contoured plug nozzle and conical plug nozzle. As the PR becomes higher, the thrust difference increases almost linearly. The advantage of the contoured plug nozzle over the conical nozzle becomes remarkable as the altitude increases. When using the contoured nozzle, roughly 5–6% thrust improvement can be achieved. The reason for the thrust improvement can be found in Fig. 16, where the pressure distributions along the nozzle surface at the PR of 500 are plotted. The contoured nozzle produces higher pressure at the radial distance of $Y = 0.3$–0.7, which contributes to the thrust increase. Although the conical plug nozzle has a higher pressure at the tip of the plug, the area and the produced pressure thrust are small. The high pressure at the tip of the conical plug nozzle is caused by the trailing shock wave formed by the interaction of the flows. From Fig. 17 flow separation

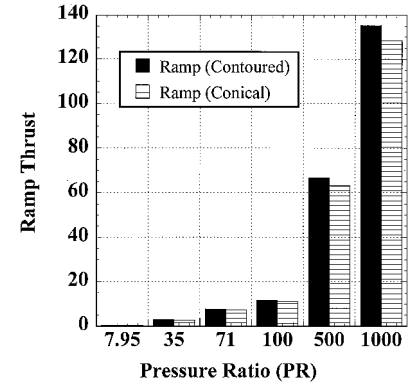

Fig. 14 Pressure thrust produced at the ramp (100% plug nozzle).

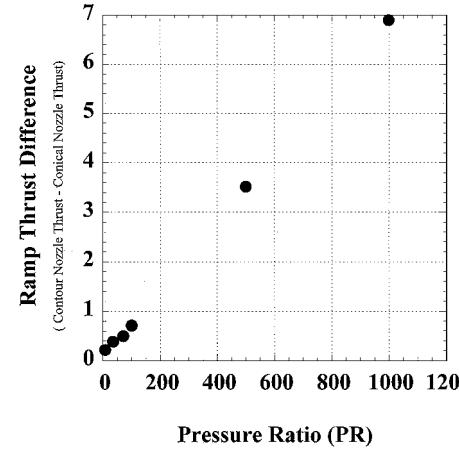

Fig. 15 Relation between contoured and conical nozzle (100% plug nozzle).

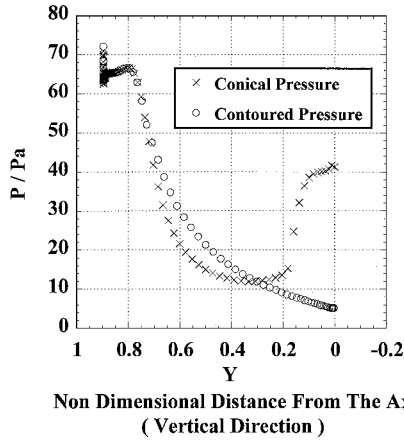

Fig. 16 Pressure distribution on the plug surface (100% plug nozzle).

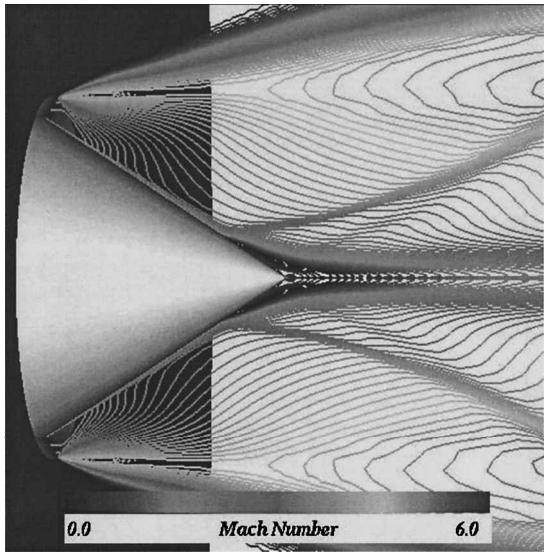

Fig. 17 Mach-number distribution on conical nozzle (PR = 500).

can be observed at the plug tip. The interaction of the boundary layer over the plug surface and the trailing shock wave induces the flow separation on the plug region and creates a high-pressure region near the tip of the conical nozzle.

Effect of the External Flow on the Nozzle Surface

Figures 18 and 19 show the comparison of the Mach-number distributions on the 100% contoured plug nozzle with and without the influence of an external flow. The PR is 500, and the external flow Mach number is 3.4. In Fig. 18 oblique shock wave is observed downstream of the boat-tail portion. The shock wave is formed by the interaction between jet plume and the external flow. At the boat-tail region a locally higher Mach-number region is observed. The external flow expands at the boat-tail region and forms a low-pressure area. The nozzle flow locally expands more strongly because of the local low ambient pressure, and the local Mach number becomes higher. The existence of the external flow also causes the barrel shock to be more inclined toward the axis.

Figure 20 shows the pressure distribution along the vehicle to the plug tip. S is the distance from the front tip of the vehicle and is nondimensionalized by the length between the axis and cowl lip. $S < 32.8$ corresponds to the vehicle region, $S = 32.8$–33.65, to the boat-tail region and $S < 33.65$, to the nozzle surface extending from the discharge to the plug tip. As was discussed in Fig. 18, the external flow expands at the corner of the vehicle and forms a low-pressure region at the boat-tail region ($S = 32.8$–33.65). If the external flow is not considered, the pressure in this area is constant and equals the external pressure. For the discharge and the plug-nozzle region

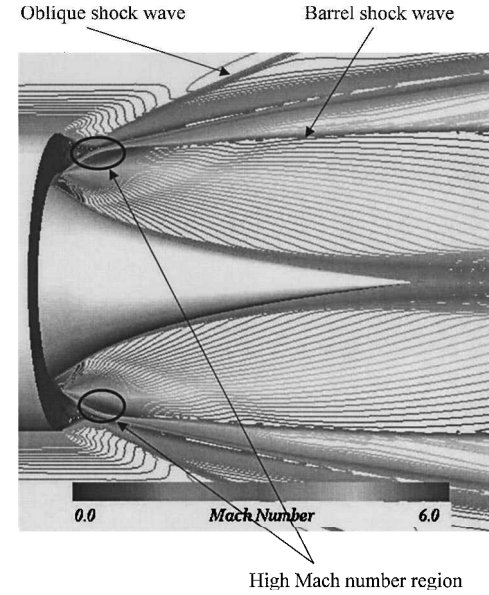

Fig. 18 Mach-number distribution with external flow (PR = 500 external mach number 3.4).

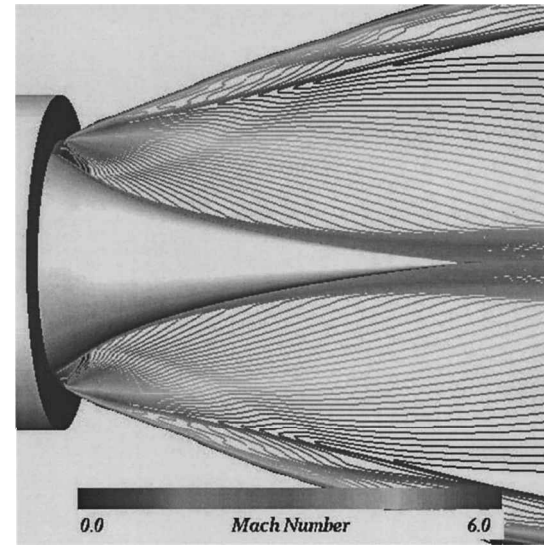

Fig. 19 Mach-number distribution without external flow (PR = 500).

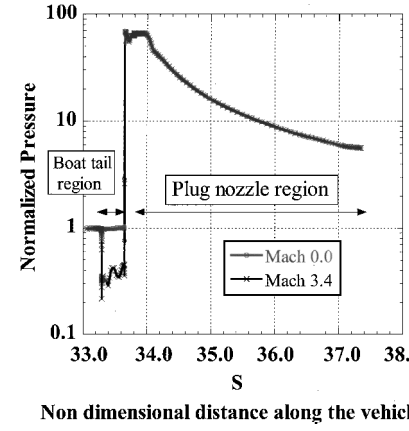

Fig. 20 Pressure distribution along the vehicle body surface.

($S > 33.65$) there is no difference in the pressure distribution, and therefore the pressure thrust produced at the nozzle surface is almost the same in both the cases. The pressure distributions with and without the external flow on the nozzle surface become the same as long as the barrel shock emanating from where the jet boundary and the external flow interact each other does not impinge on the nozzle surface. The last characteristic line emanating from the cowl lip reaches the plug tip at the designed point (PR = 71). When the external flow exists, the jet expands to the local low-pressure region at the boat tail and makes the last characteristic line (which leads to the barrel shock wave) to impinge further downstream of the plug tip. This shows that the external flow does not influence the pressure distributions on the nozzle surface when the PR is higher than the designed point.

Conclusions

The flow structure and the performance of the plug nozzle are numerically investigated. The results clearly showed the main advantages of the plug nozzle. The thrust is close to the theoretical value at the entire altitude and almost insensitive to truncation of the nozzle length. Thrust reduction caused by the cut of the nozzle is compensated by the thrust gained by the base pressure. It has turned out that the base pressure is equal to the ambient pressure at low altitudes (e.g., low chamber-to-ambient PRs), and it does not produce thrust, while it takes almost constant value at high altitudes (e.g., high chamber-to-ambient PRs) and contributes to the total thrust. The external flow over the plug nozzle does not influence the pressure distributions over the plug surface when the PR is higher than the designed point. The pressure thrust produced at the nozzle surface is not altered whether the external flow is considered or not.

Acknowledgment

This work was partly financed by the Japan Society for the Promotion of Science (Project 12-07301). The first author would like to appreciate their support.

References

[1]Hagemann, G., Immich, H., and Terhardt, M., "Flow Phenomena in Advanced Rocket Nozzles—The Plug Nozzle," AIAA Paper 98-3522, July 1998.

[2]Immich, H., Nasuti, F., Onofri, M., and Caporicci, M., "Experimental and Numerical Analysis of Linear Plug Nozzles," AIAA Paper 98-1603, April 1998.

[3]Rommel, T., Hagemann, G., Schley, C. A., Krulle, G., and Manski, D., "Plug Nozzle Flowfield Analysis," *Journal of Propulsion and Power*, Vol. 13, No. 5, 1997, pp. 629–634.

[4]Fick, M., "Performance Modeling and Systems Aspects of Plug Cluster Nozzles," AIAA Paper 98-3525, July 1998.

[5]Nasuti, F., and Onofri, M., "Methodology to Solve Flowfields of Plug Nozzles for Future Launchers," *Journal of Propulsion and Power*, Vol. 14, No. 3, 1998, pp. 318–326.

[6]Tomita, T., Tamura, H., and Takahashi, M., "An Experimental Evaluation of Plug Nozzle Flow Fields," AIAA Paper 96-2632, July 1996.

[7]Tomita, T., Takahashi, M., and Tamura, H., "Flow Field of Clustered Plug Nozzles," AIAA Paper 97-3219, July 1997.

[8]Ruf, J. H., and McConaughey, P. K., "A Numerical Analysis of a Three Dimensional Aerospike," AIAA Paper 97-3217, July 1997.

[9]Lee, C., and Thompson, D., "Fortran Program for Plug Nozzle Design," NASA TM X-53019, July 1964.

[10]Shima, E., and Jounouchi, T., "Role of CFD in Aeronautical Engineering (No14)—AUSM Type Upwind Schemes," *Proceedings of the 14th NAL Symposium on Aircraft Computational Aerodynamics*, National Aerospace Laboratory, SP-34, Tokyo, Japan, 1997, pp. 7–12.

[11]Baldwin, B. S., and Lomax, H., "Thin Layer Approximation and Algebraic Model for Separated Turbulent Flows," AIAA Paper 78-257, Jan. 1978.

[12]Degani, D., and Schiff, L. B., "Computation of Turbulent Supersonic Flows around Pointed Bodies Having Crossflow Separation," *Journal of Computational Physics*, Vol. 66, No. 1, 1986, pp. 173–196.

[13]Fujii, K., "Practical Applications of New LU-ADI Scheme for the Three-Dimensional Navier–Stokes Computation of Transonic Viscous Flows," AIAA Paper 86-0513, Jan. 1986.

[14]Paciorri, R., Nasuti, F., and Sabetta, F., "Evaluation of Turbulence Modeling in Supersonic Afterbody Computations," AIAA Paper 2001-3039, June 2001.

[15]Spalart, P. R., and Allmaras, S. R., "A One-Equation Turbulence Model for Aerodynamic Flows," AIAA Paper 92-0439, Jan. 1992.

[16]Sykes, D. M., "Cylindrical and Boat-Tailed After-Bodies in Transonic Flow with Gas Ejection," *AIAA Journal*, Vol. 8, No. 3, 1970, pp. 588–590.

[17]Herrin, J. L., and Dutton, J. C., "Supersonic Base Flow Experiments in the Near Wake of a Cylindrical Afterbody," *AIAA Journal*, Vol. 32, No. 1, 1994, pp. 77–83.

[18]Seiling, W. R., and Page, R. H., "A Re-Examination of Sting Interference Effects," AIAA Paper 70-585, May 1970.